RSC Advances

ROYAL SOCIETY OF CHEMISTRY

www.rsc.org/advances

RSC Advances

RSCPublishing

PAPER

Development of organically modified silica nanoparticles for monitoring intracellular level of oxygen using frequency-domain FLIM platform

Cite this: DOI: 10.1039/x0xx00000x

Received 3rd December 2014,
Accepted ooth xx xxxx

DOI: 10.1039/x0xx00000x

http://www.rsc.org/Advances

Barbara Korzeniowska*[a] , Marcel Raspe[b] , Dorota Wencel[a] , Robert Woolley[a] , Kees Jalink[b] and Colette McDonagh[a]

Abstract Monitoring cellular homeostasis is one of the crucial elements in understanding the real causes of the pathological state and in designing more efficient treatments. Fluorescent nanometer sized particles have great potential in the quantitative real – time analysis of important cellular analytes. In this paper we focus on the development of optical chemical nanosensors for probing dissolved oxygen inside living cells. The nanosensor is composed of organically modified silica nanoparticles, doped with the luminescent oxygen – sensitive [Ru(II)-tris(4,7-diphenyl-1,10-phenanthroline)] ($[Ru(dpp)_3]^{2+}$) complex. A monodisperse population of nanoparticles with average size of 70 nm was obtained based on a modified sol-gel-based Stöber method. The nanoparticles were initially calibrated in water using a phase fluorometry setup. Very good repeatability from cycle to cycle and reversibility in oxygen response was obtained for nanoparticles. The excellent performance of the nanosensors is reflected in their very low limit of detection (LOD) (0.007 ppm). Transmission electron microscopy images obtained from in vitro studies reveals that the final intracellular location of the nanoparticles is in the lysosomes. The performance of the nanoparticles was tested inside cells using Fluorescence Lifetime Imaging Microscopy (FLIM) instrumentation. Despite a decrease in the oxygen sensitivity of nanoparticles located in the intracellular milieu (LOD = 0.226 ppm), a significant change in lifetime (~1.3 μs) is detected within the physiological oxygen concentration range. Moreover, nanoparticles show no cytotoxic effect when incubated with cells for up to 72 h. These results demonstrate therefore the great potential of ($[Ru(dpp)_3]^{2+}$) – doped organically modified silica nanoparticles for monitoring the intracellular oxygen concentration.

Introduction

Real-time, non-invasive monitoring of events occurring at the cellular level is of great importance for early diagnosis, effectiveness of therapy and for design of new therapeutic agents. Among different parameters, oxygen is one of the most important analyte of interest, due to its participation in crucial cellular metabolism processes including production of ATP in oxidative phosphorylation route as well as synthesis of reactive oxygen species (ROS),[1] nitric oxide (NO),[2] ionic gradients[3] and transcription factors.[4] Information about the oxygen levels and cellular respiration kinetics could then be used to detect any abnormalities occurring within the intracellular milieu, which could contribute a better understanding of many 21st century diseases including cancer, diabetes as well as Alzheimer's, Parkinson's and cardiovascular disorders.[5]

The level of oxygen can be measured by several different techniques. The traditional detection methods such as Winkler titration[6] and Clarke electrode[7] are, due to their time and analyte consuming nature, inappropriate for intracellular measurements. A technique which overcomes these limitations is based on the optical detection of the luminescence signal, using a dye which is gradually quenched with increasing amount of oxygen.[8] Obtaining quantitative data from intracellular studies is very challenging, especially for fast diffusion of dissolved oxygen through the cellular membrane. To date, at least two different optical sensing approaches have been used to quantify the concentration of oxygen inside the cells. The first technique, applicable to standard fluorescence microscopes, is based on the measurement of intensity ratio (excitation or emission peaks), where one is dependent and another one is independent of the analyte concentration. Some examples of this approach with different luminophore pairs co-encapsulated in various oxygen-sensitive nanoparticle matrices (i.e. ruthenium (II) complex with Oregon Green 488 – dextran in silica nanoparticles,[9] platinum (II) complex with octaethylporphine in the organically modified silicates (ORMOSILs) nanoparticles[10] and in polymer nanoparticles[11] as well as conjugate of palladium (II) complex with dendrimer (G2) and Alexa 647 – dextran in polymer nanoparticles[12]) have

been reported in the literature. The second technique, which can be applied to intracellular oxygen studies, employs the luminophore lifetime and it requires more advanced Fluorescence Lifetime Imaging Microscopy (FLIM) instrumentation. Two different optical detection techniques, Time Correlated Single Photon Counting (TCSPC) and phase-fluorometry implemented in time-domain and frequency-domain (FD) mode, respectively, are currently widely used for fluorescence lifetime measurements. In the time-domain mode, the sample is excited with a pulsed excitation source and then the luminescence lifetime decay is reconstructed in time. The frequency-domain mode uses a modulated light source to excite the sample. The luminescence lifetime is then calculated from the phase delay and modulation ratio of the emission relative to the excitation. The lifetime-based measurements are insensitive to many interfering factors such as dye concentration, photobleaching, as well as variation in excitation source intensity, gain of the detector, signal loss within the optical path or specimen, and microscope focusing. Therefore FLIM is considered to be more reliable in the field of intracellular imaging and sensing, where equal distribution of dye across the biological specimen is very challenging if not impossible to achieve. Luminescent ruthenium (II) and phosphorescent platinum (II), palladium (II) and iridium (III) complexes due to their long-lifetimes in the range, from a few microseconds up to hundreds of milliseconds, are very suitable for the quantitative measurements of oxygen. The very long acquisition times required for the collection of photons emitted from these long-lifetime oxygen-sensitive luminophores exclude the application of time-domain FLIM for quantitative oxygen studies. In contrast, FD FLIM has been shown to be a very efficient tool for monitoring cellular respiration processes.[13] Different types of oxygen-sensitive probes have been developed including dyes conjugated with cell penetrating peptides,[14] PEGylated dendrimers[15] as well as nanoparticles containing one or more luminophores.[16,17] Nanoparticles, in particular, have great potential for monitoring of the intracellular environment due to their flexibility in the design, which facilitates multianalyte[18,19] and/or multimodal detection.[20,21] By embedding the luminophores within the nanoparticle matrix, the possibility of non-specific binding between proteins and molecules of the indicator dye as well as potentially toxic interactions between the cellular components and the organic compound are minimised. Due to their small dimension (20-600 nm), the spherical nanosensors occupy from 1 ppm to 1 ppb of the mammalian cell volume, which make them relatively non-invasive and can help them evade the immune system. Other important features of nanoparticles include the high loading efficiency of dye resulting in signal amplification and capability of targeting of the nanoparticle to the location of interest by coating their surface with proteins and peptides.[22] The nanoparticle sensing concept, introduced to the literature by the Kopelman group over 10 year ago as probes encapsulated by biologically localized embedding (PEBBLEs),[23] was successfully applied for the detection of many intracellular analytes such as O_2,[9,10] pH,[24-26] Ca^{2+},[27-29] Cl^-,[30] Zn^{2+},[19,31,32] Cu^{2+} [33-35] and H_2O_2[36,37] as well as for a cell labeling.[38,39] Among different types of available approaches including polymer[40] and magnetic[41] nanoparticles, quantum dots[42] and carbon nanotubes,[43] silica nanoparticles are very attractive candidates for cellular sensing. The versatile chemistry of silica and the negative charge on the nanoparticle surface allow for tailoring of the nanoparticle properties such as porosity, hydrophobicity and colloidal stability. In addition, the silica nanoparticles can be easily conjugated with different bio-recognition agents (i.e. antibodies,[44] protein complexes,[45] nucleic acids[46]) for more efficient cell loading and cell staining. Other beneficial properties of silica nanoparticles include their optical transparency, enhanced dye photostability[47,48] and relative biocompatibility.[49,50]

Here we present a new oxygen-sensitive probe composed of organically modified silica nanoparticles, an organic-inorganic hybrid material, in which the organic component derived from methyltriethoxysilane (MTEOS) was chemically bonded to the silica matrix which was doped with the luminescent ($[Ru(dpp)_3]^{2+}$) complex. Nanoparticles with a size compatible for the intracellular studies (around 70 nm in diameter) are synthesised using a modified Stöber method. The nanosensor performance is tested first in water using phase fluorometry and then inside Human Osteosarcoma Epithelial (U_2OS) cells with wide-field FD FLIM. In addition, results from the detailed studies on the nanoparticle intracellular localisation are presented. Finally, the biocompatibility of these nanoparticles was tested using a standard colorimetric cytotoxicity assay.

Results and discussion

Nanoparticle synthesis

Nanoparticles were synthesised using a modified Stöber method. As reported in the literature, the introduction of organic groups into the silica network, improves significantly its oxygen sensitivity.[51] Nanoparticle synthesis was therefore initiated by hydrolysis and condensation of TEOS under basic conditions, which then was followed by the addition of pre-hydrolysed MTEOS after 6 h of the reaction. This preliminary hydrolysis and condensation of the ORMOSIL was carried out outside of the reaction vial in an acidic environment. The luminescent $[Ru(dpp)_3]Cl_2$ complex was added as well at this stage to the forming nanoparticles. Due to its positive charge, $[Ru(dpp)_3]Cl_2$ can be easily entrapped within the negatively charged nanoparticle silica matrix using electrostatic interactions. In addition, the lack of solubility of $[Ru(dpp)_3]Cl_2$ in water eliminates the risk of dye leaching out of the nanoparticle structure, which results in a good compatibility of $[Ru(dpp)_3]Cl_2$ - doped nanoparticles for the intracellular studies. A general scheme of this modified Stöber synthesis is presented in Figure 1.

Fig. 1 Schematic of the modified Stöber-based nanoparticle synthesis. The synthesis initiates with hydrolysis and condensation of TEOS, which is then followed by addition of prehydrolysed MTEOS (mixed with $[Ru(dpp)_3]^{2+}$ stock solution) after 6 h of the reaction. After 24 h of the synthesis, nanoparticles are centrifuged and washed in EtOH. The sample after purification (see photo) is transferred into water and kept at 4^0C protected from light.

TEM images, shown in Figure 2, revealed a spherical, monodispersed population of nanoparticles with an average diameter of 65 nm ± 7.8 nm.

Fig. 2 TEM results. The average size of nanoparticles is 65 nm ± 7.8 nm (dried sample).

The average hydrodynamic diameter of nanoparticles and a Polydispersity Index (PDI) obtained from Dynamic Light Scattering (DLS) measurements were equal to 90.6 nm ± 17.8 nm and 0.035, respectively (see Figure S1). The zeta potential

of nanoparticles is equal to -40 mV. A small PDI value and high zeta potential of nanoparticles indicates their good monodispersity and excellent colloidal stability in aqueous solution, respectively. However, when nanoparticles are transferred into the phosphate buffered saline (PBS) or into the serum-containing cell culture media at the same concentration as then used in the experiments with cells, significant aggregation of nanoparticles and drop in the zeta potential occurs within first 48h (see Table S1).

Optical properties and calibration of nanoparticles

Spectrofluorometric characterisation of the nanoparticles was performed prior to the nanosensor calibration. The excitation and emission spectra of nanoparticles were compared to the spectra of pure $Ru(dpp_3)^{2+}$ complex. As can be observed in Figure 3, there was a small shift (~10 nm) toward the longer wavelengths observed in the emission spectrum of nanoparticles dispersed in water (the emission peak at 610 nm) with respect to the one obtained for the free $[Ru(dpp)_3]Cl_2$ dissolved in EtOH. This small spectral variation very likely derives from the difference in the fluorophore microenvironments (EtOH versus organically modified silica nanoparticles in water), which has been reported in the literature as a factor influencing the optical properties of the dye.[52]

Fig. 3 Normalised excitation and emission spectra of $[Ru(dpp)_3]^{2+}$ (λ_{exc} = 450 nm, λ_{em} = 610 nm) (in black) and of the complex entrapped in sol–gel nanoparticles (in red). The dash dot and the solid lines correspond to the excitation and the emission spectra of the fluorophore, respectively.

Then, nanosensors were calibrated in water using the phase fluorometry setup. Changes in the phase angle ϕ, a parameter related to the luminophore lifetime τ and the modulation frequency f (see Eq. 1), were recorded in time under different oxygen concentrations (from 0 % to 100 %) and are presented in Figure 4a.

$$\tau = \frac{tan\phi}{2\pi f}, \quad (1)$$

Due to the dynamic quenching process, where excited dye molecules collide with oxygen and return to their ground state without photon emission, under increased oxygen concentrations a decrease in the overall luminescence intensity and lifetime as well as the phase angle occurs. The nanoparticles show excellent repeatability from cycle to cycle and reversibility.

The overall quenching response of the nanosensor to dissolved oxygen (Q_{DO}) can be calculated based on the Eq. 2:

$$Q_{DO} = \frac{\phi_{N_2} - \phi_{O_2}}{\phi_{N_2}} \cdot 100\%, \quad (2)$$

where ϕ_{N_2} and ϕ_{O_2} are phase angles in fully deoxygenated and oxygenated water, respectively. The measured value of Q_{DO} for the $[Ru(dpp)_3]Cl_2$ - doped organically modified silica nanoparticles is 75%, which is in the range of values reported in the literature for ORMOSIL films.[51] The quenching process can be described by different models. In a homogeneous environment, the dependence of I_0/I or τ_0/τ versus pO_2 is represented as a straight line with a vertical intercept at 1 and slope equal to Stern Volmer constant (K_{SV}), which is used then as a value describing sensor sensitivity. In a lot of cases, microenvironment variations leads to different local quenching profiles, for which other non-linear models have been established.[53-55]

Fig. 4 a) Phase fluorometry response of nanoparticles doped with $[Ru(dpp)_3]^{2+}$ monitored within full (from 0 ppm to 42.5 ppm) dissolved oxygen concentration range. Number of cycles is equal to 3. **b)** best fit to the Stern-Volmer and Demas model for the data corresponding to the physiological dissolved oxygen concentration range (from 0 ppm to 9 ppm).

In general terms, when two different microenvironments with Stern-Volmer constants K_{SV1} and K_{SV2} are present in the luminophore-doped sensing matrix, the two-site Demas model can be applied to describe the quenching processes. It is to be noted that this model also fits well to a broad heterogeneous distribution of slightly different microenvironments. In this work, the data obtained on the phase fluorometry setup was fitted to the linear Stern-Volmer (see Eq. 3) and non-linear Demas (see Eq. 4) models in order to obtain the calibration plots (Figure 4b). The dissolved oxygen concentrations, expressed in ppm, were calculated based on the solubility constant of oxygen in water at 21°C (0.004252 g of O_2 in 100 g of H_2O).[9] The fitting was performed only for the data contained within the physiological dissolved oxygen concentration range (0 ppm – 9 ppm).

$$\frac{I_0}{I} = \frac{\phi_0}{\phi} = \frac{\tau_0}{\tau} = 1 + k_q \tau_0 \cdot pO_2 \quad (3)$$

$$\frac{I_0}{I} = \frac{\phi_0}{\phi} = \frac{\tau_0}{\tau} = \left[\frac{f_1}{1+K_{SV1}\cdot pO_2} + \frac{f_2}{1+K_{SV2}\cdot pO_2}\right]^{-1} \quad (4)$$

where:

$\boldsymbol{I_0, I}$ - the luminescence intensity of the luminophore in the absence and presence of O_2

$\boldsymbol{\tau_0, \tau}$ - the luminescence lifetime of the luminophore in the absence and presence of O_2

$\boldsymbol{K_{SV}}$ - Stern-Volmer constant

$\boldsymbol{pO_2}$ - partial pressure of O_2

$\boldsymbol{k_q}$ - bi-molecular quenching constant

$\boldsymbol{f_i}$ - fractional contribution to the total emission from site i

$\boldsymbol{K_{SVi}}$ - discrete Stern-Volmer constant associated with site i

Table 1. Stern-Volmer and Demas fitting parameters for the $[Ru(dpp_3)]^{2+}$-doped organically modified silica nanoparticles calibrated in water

Stern Volmer model			
K_{SV}		r^2	
0.1171 ± 0.0037		0.987	
Demas model			
f_1	K_{SV1}	K_{SV2}	r^2
0.61 ± 0.06	0.2281 ± 0.0178	0.0331 ± 0.0079	0.999

K_{SV} - Stern-Volmer constant, K_{SVi}- discrete Stern-Volmer constant associated with site i, f_i - fractional contribution to the total emission from site i, r^2-regression

The Demas model gave an excellent correlation with the data (r^2=0.999) (see data in Table 1) which, as noted above, can be interpreted as the presence of a heterogenous microenvironment around the $[Ru(dpp)_3]^{2+}$) molecules. Further inspection of the data

from Table 1 reveals that a larger fraction (~61%) of ($[Ru(dpp)_3]^{2+}$) molecules are located in the microenvironment permeable to the oxygen. A good fit was also obtained for the Stern-Volmer model (r^2=0.987). In addition, small error bars presented for the calibration curves (n = 3) indicate excellent nanoparticle batch to batch reproducibility. The sensing performance of nanoparticles in water was evaluated by calculating the limit of detection (LOD, calculated as three times the standard deviation (3σ)) of the nanosensor (in the range 0-9 ppm) which is equal to 0.007 ppm. The response time of the nanosensor was in the range from 150 s (for 0 ppm) up to 130 s (for 9 ppm).

Nanoparticle intracellular trafficking

Due to the limitation of optical microscopy in resolving the objects smaller than a few hundred nm, an investigation on the intracellular localisation of nanoparticles was performed using the Transmission Electron Microscopy (TEM) technique. The images obtained from this analysis, presented in Figure 5, indicate that the nanoparticles are transported inside the cell through the endosomal lysosomal pathway.

An increase in the average amount of the nanoparticles per lysosome N, can be observed in time (3 and 10 for 12 h and 24 h incubation sample, respectively). In addition, comparison of TEM images of the pure nanoparticles dried on the grids (Figure 2a) and the ones uptaken by cells (Figure 5b, c) revealed no difference in the nanoparticle structure. This suggests that the nanoparticles do not undergo the enzymatic processes occurring under low lysosomal pH (~4-5) within a first 48 h of the incubation.

Fig. 5 TEM of cells with nanoparticles **a)** negative control, **b)** 24 h nanoparticle incubation, **c)** 48 h nanoparticle incubation samples. Nanoparticles (dark rounded spots) are located in the lysosomes (oval dark grey structures). An increase in the amount of nanoparticles per lysosome is observed with longer incubation time. Scale bar: 1 µm.

Nanoparticle intracellular calibration

Intracellular calibration of nanoparticles was performed using a FD FLIM setup. Adherent U_2OS cell line derived from the osteosarcoma disease was reported in the literature as a good tumor model[56] and was used in this study. As presented in Figure 6a, upon introducing oxygen into the media, the long lifetime of $[Ru(dpp)_3]Cl_2$ - doped nanoparticles (indicated in orange) drops down from around 4.4 µs to 3.3 µs, what is associated with quenching of the luminescence signal derived from the luminophore (indicated in blue). Based on these results, the calibration plot was then drawn and fitted to a linear Stern-Volmer and a non – linear Demas two – site model (see Eq. 4) within the physiological dissolved oxygen concentration range as presented in Figure 6b.

Fig 6 FD FLIM–based calibration of $[Ru(dpp_3)]^{2+}$-doped organically modified silica nanoparticles performed inside respiring U_2OS cells **a)** Lifetime images and time course data and **b)** corresponding calibration curve (n=3). Color scale corresponds to the lifetime of $[Ru(dpp_3)]^{2+}$.

A poor fit to the linear model (r^2=0.892) was obtained for nanoparticles uptaken by cells very likely caused by the more heterogeneous environment present in the cell. In comparison, the Demas model gave an excellent correlation with the data (r^2 = 0.999) (see data in Table 2) indicating the presence of two microenvironments with different oxygen accessibility within nanoparticle matrix. The fitting parameters obtained for the Demas model demonstrate a decrease (~44%) in a population of $[Ru(dpp)_3]Cl_2$ molecules located in the domain with higher oxygen accessibility when nanoparticles are calibrated inside the cells (f_1=0.34, Table 2) instead of in water (f_1=0.61, Table 1). This decreased availability of dye molecules to oxygen quenching may be caused by a physical adsorption of proteins present in the cellular media to the nanoparticle surface as previously reported in the literature.[57]

Table 2. Stern-Volmer and Demas fitting parameters for the $[Ru(dpp_3)]^{2+}$-doped organically modified silica nanoparticles calibrated inside U_2OS cells

Stern Volmer model			
K_{SV}		r^2	
0.0504 ± 0.0037		0.892	
Demas model			
f_1	K_{SV1}	K_{SV2}	r^2
0.34 ± 0.07	0.3165 ± 0.0762	0.0046 ± 0.0061	0.999

K_{SV} - Stern-Volmer constant, K_{SVi}- discrete Stern-Volmer constant associated with site i, f_i - fractional contribution to the total emission from site i, r^2-regression

The intracellular dissolved oxygen value obtained from the calibration curve for respiring cells at normoxic condition (8.5 ppm) was equal to be 7.8 ppm what is in agreement with previously published data.[10] Despite the higher limit of detection (LOD = 0.226 ppm) in comparison to that obtained for nanosensors dispersed in water, the results demonstrate that quantitative intracellular measurements can be performed using this FD technique.

Cytotoxicity studies

Nanoparticle cytotoxicity was evaluated based on a cell proliferation assay. This colorimetric method is based on the reduction of 5-[3-(carboxymethoxy)phenyl]-3-(4,5-dimethyl-2-thiazolyl)-2-(4-sulfophenyl)-2H-tetrazolium inner salt (MTS) to a formazan (λ_{abs} = 490 nm) by cellular enzymes. Cell viability can be therefore estimated by a simple absorbance measurement. To verify whether $[Ru(dpp)_3]Cl_2$ - doped organically modified silica nanoparticles are cytotoxic, U_2OS cells were exposed to different concentrations of nanoparticles for 72 h and the absorbance values at 490 nm were then recorded and plotted (see Figure 7).

Fig. 7 Cytotoxicity data obtained for U_2OS cells incubated for 72 h with different amounts of $[Ru(dpp_3)]^{2+}$-doped organically modified silica nanoparticles.

Differences between samples were assessed using one – way ANOVA statistical analysis which revealed no cytotoxic effect even for higher nanoparticle concentrations. A very crucial feature of the intracellular nanosensor, very good biocompatibility, was confirmed for these newly developed oxygen-sensitive nanoparticles.

Experimental

Chemicals and materials

Absolute ethanol (EtOH), 28% (v/v) ammonium hydroxide solution (NH_4OH), 0.1 M hydrochloric acid (HCl), tetraethoxysilane (TEOS), methyltriethoxysilane (MTEOS), ruthenium-tris(4,7-diphenyl-1,10-phenanthroline) dichloride ($[Ru(dpp)_3]Cl_2$), sodium chloride (NaCl), potassium chloride

(KCl), magnesium chloride ($MgCl_2$), calcium chloride ($CaCl_2$), glucose, Dulbecco's Modified Eagles Medium (DMEM) and 4-(2-Hydroxyethyl)piperazine-1-ethanesulfonic acid (HEPES) were obtained from Sigma Aldrich, Ireland. 200 and 300 mesh copper grid with formvar/carbon film, uranyl acetate, lead citrate were purchased from Agar Scientific, UK. Glutaraldehyde was acquired from BDH Laboratory Supplies, UK. Monobasic and dibasic sodium phosphate (NaH_2PO_4 and Na_2HPO_4) were supplied by Riedel-deHaën AG, Seelze, Germany. Osmium tetroxide (OsO_4) was purchased from Oxkem Limited, UK. EtOH:epoxy resin was obtained from Epon, UK. 50 ml plastic centrifuge tubes and sodium hydroxide (NaOH) were obtained from VWR, Ireland. Plastic tubing and a silicone stopper were purchased from Tygon, USA and Cole-Parmer Instruments, Japan, respectively. CellTiter 96® Aqueous One Solution Reagent was acquired from Promega, Ireland. 6-, 12- and 96-well plates were purchased from Nunc™, USA. 35 mm plastic petri dishes were supplied from SARSTEDT, USA. T-75 flasks were obtained from Fisher Scientific, UK. Penicillin-Streptomycin, phosphate buffered saline (PBS) and fetal bovine serum (FBS) were purchased from GIBCO, Ireland. Glass coverslips were acquired from Deckgläser, Germany. Sterile deionised (DI) water was used for the preparation of an aqueous nanoparticle solution. All chemicals were of analytical grade and were used without further purification.

Fabrication of the nanoparticles

The nanoparticles were fabricated based on an optimised modified Stöber synthesis.[58] The nanoparticle formation was initiated in a basic environment in the following way: 0.5 ml of TEOS was mixed on the stirrer with 12.2 ml of EtOH for 15 minutes and then a reaction catalyst, NH_4OH, was added dropwise to the reaction mixture in the amount of 0.75 ml. In the second step of the synthesis, implemented with 6 h time delay with respect to the beginning of TEOS hydrolysis, the pH of the reaction mixture was decreased upon addition of HCl. In parallel, a second prehydrolysed silica precursor, MTEOS, was introduced into the reaction mixture. Initial hydrolysis and condensation of MTEOS occurred outside of the main reaction vial according to following protocol: 2.86 ml of MTEOS was mixed with 3.24 ml of $[Ru(dpp)_3]^{2+}$ stock solution (2 mg/ml in EtOH) and 2.02 ml of EtOH. After 15 minutes, 1.037 ml of HCl was added dropwise to initiate the hydrolysis of MTEOS. In another 15 minutes time interval, 0.5 ml of the mixture containing prehydrolysed MTEOS was pipetted into the reaction vial. The reaction mixture was left on the stirrer for another 20 hours at room temperature. The nanoparticles were collected by centrifugation (8320 rcf, 30 min) and resuspended in EtOH using ultrasonication, which was followed by three washing steps in EtOH (7 ml). The sample after washing was re-suspended in water and kept in the dark under ambient conditions. Just before performing the intracellular uptake and sensing experiments, the nanoparticles were sterilised by one wash in EtOH and then re-suspended in sterile DI water.

Nanoparticle characterisation

DLS

The measurements of nanoparticle size and zeta potential were done using a Delta™NanoC Particle Analyzer (Beckman Coulter, USA) equipped with two 30 mW 658 nm laser diodes as light sources, designed for separate size and zeta potential measurements. Aqueous solutions of the nanoparticles at the concentration of 4 mg/ml were prepared for the analysis. Polydispersity Index (PDI) values were calculated from size distribution data of each nanoparticle population. Each value reported was an average of five measurements.

TEM

Ethanol solutions of the nanoparticles at a concentration of 1 mg/ml were dried on a 300 mesh copper grid with formvar/carbon film. Images were acquired using a Tecnai G2 20 Twin microscope (FEI, USA).

Spectrofluorometry

The luminescence excitation and emission spectra of the nanoparticles were recorded using a FluoroMax-2 spectrofluorometer (Horiba Jobin Yvon, USA) equipped with a continuous wave 150 W xenon lamp as a light source. The stock solution of the nanoparticles in DI water were diluted (10x) and transferred into a quartz cuvette for standard excitation and emission spectra measurements. The excitation and emission spectra were collected at 610 nm and 450 nm (3 nm bandwidth), which corresponds to ($[Ru(dpp)_3]^{2+}$) emission and excitation peaks, respectively.

Nanosensor calibration

The oxygen-sensitivity of the nanoparticles was tested using a phase fluorometry-based oxygen reader (DELTA, Denmark) which consisted of an optical fibre, a 450 nm blue LED modulated at an optimal frequency of 20 kHz for ($[Ru(dpp)_3]^{2+}$) , a red filter (DELTA, Denmark) and a photodiode detector. Oxygen (O_2) and nitrogen (N_2) gases (BOC, Ireland) were mixed using mass flow controllers (Celerity, Ireland) and a control unit (National Instruments, Ireland) in order to obtain the gases for the calibration containing different amount of O_2 (0%, 2%, 5%, 8%, 10%, 20%, 50%, 100%). Both the mass flow controller and the oxygen reader were operated through the data acquisition and control software developed in Lab VIEW™ (National Instruments, USA). An air-tight chamber was composed of a 50 ml plastic centrifuge tube, plastic tubing and a silicone stopper with two needles providing an inlet and an outlet for bubbling the gases through the sample. Both the chamber with an aqueous solution of the nanoparticles at the concentration of 7 mg/ml and an optical fibre (attached to the bottom of the plastic tube) were placed in a holder with a clamp for the measurements. Degassing steps lasted 5 min, except the first one (0% O_2), which duration was set for 10 min in order to ensure complete removal of oxygen from the nanoparticle solution. The measurement was done every 3s.

Cellular experiments

Cell Culture

Human Osteosarcoma Epithelial (U_2OS) cells were cultured in DMEM supplemented with 10% v/v FBS and 1% v/v Penicillin-Streptomycin. Cells were maintained between 80% and 90% confluence, at low passage number (below 40) in T-75 flasks at 37 ^oC, 5% CO_2.

Intracellular trafficking

Intracellular location of nanoparticles was investigated using the TEM technique. Cells were plated at a density of $1x10^5$ cells/well in a 12-well plate. After 24 h and 48 h, nanoparticles were added to the wells for 48 h and 24 h incubation time, respectively, at a concentration of 50 μg/ml. As a negative

control, cells grown in the media without nanoparticles were prepared. Cells were washed 3 times in PBS and fixed in 2.5% glutaraldehyde in 0.1 M Sørensen's phosphate buffer (40.5 ml of 0.1M Na_2HPO_4, 9.5 ml of 0.1M NaH_2PO_4) for a minimum of 2 h at room temperature. Further sample processing steps included: post fixing in 1% of OsO_4 in DI water for 1 h at room temperature and dehydration in increasing concentrations of EtOH (30%, 50%, 70%, 90%, 100%). The samples were then immersed in an EtOH:epoxy resin (1 : 1 v / v) mixture for 1 h and transferred in pure epoxy resin for embedding, initiated at 37 ^oC (2 h) and finalised at 60^oC (24 h). Ultrathin (80 nm) sections were prepared using a Leica EM UC6 ultramicrotome (Leica Microsystems, Germany), mounted on a 200 mesh thin bar copper grids and stained with 2% uranyl acetate in DI water and 0.4% lead citrate prepared with 10% of 1M NaOH and DI water. The grids were examined in a Tecnai G2 12 BioTWIN TEM (FEI, USA) using an accelerating voltage of 120 kV. Cells were approximately 70% confluent when experiments were performed.

Intracellular sensing

Cells were grown on ultraviolet sterilized 24 mm round glass coverslips placed in a 6-well plate at a density of $1.5x10^5$ cells/well. Nanoparticles were applied into the media above the cells, after 24 h incubation time, at the concentration of 50 µg/ml. Cells were incubated for another 48 h before performing the intracellular oxygen-sensing experiments. The coverslips were washed 3 times in PBS and transferred into a coverslip holder, Attofluor® Cell Chamber (Invitrogen, The Netherlands) containing 500 µl of preheated (37 °C) HEPES buffered saline (140 mM NaCl, 5 mM KCl, 1 mM $MgCl_2$, 1 mM $CaCl_2$, 10 mM glucose and 10 mM HEPES) pH 7.4. Calibration gas mixtures with different amounts of O_2 (0%, 4%, 8%, 12%, 16%, 20%) were generated using mass flow controllers (Bronkhorst Hi-Tec, The Netherlands) and delivered through plastic tubing to a chamber composed of a 35 mm plastic petri dish, placed on the top of the coverslip holder, and end of a 2-200 µl standard plastic tip, punched into the petri dish wall, acting as tubing inlet for the gases. The FD FLIM images were acquired using Lambert Instruments hard- and software and a DMIRE2 widefield microscope (Leica, Germany) equipped with a 1W 473 nm LED modulated at 100 kHz, I3 filter cube (450-490 nm band pass excitation filter, 510 nm dichroic mirror, 515 nm long pass emission filter) and a 63x glycerine immersion objective (Leica HCX PL APO 370C, na =1.3). Excitation light was collected with a frequency-modulated image intensifier, II18MD (Lambert Instruments, The Netherlands) coupled to a charge-coupled device camera, CCD-1300D (VDS Vosskuhler, Germany). CCD camera (Vosskuhler CCD - 1300D) was used. In order to reach an equilibrium between intra- and extra-cellular oxygen concentrations degassing steps duration was set at 3 min. The measurement was done every 15 s and the cells were kept at 37^oC during image acquisition.

Cytotoxicity studies

Toxicity of nanoparticles was investigated using a colorimetric cell proliferation assay, CellTiter 96® Aqueous One Solution Reagent, in accordance with the manufacturer's instructions. Briefly, $2.5x10^3$ cells/well were plated in a 96-well plate. After 4 hours, nanoparticles were added to final concentrations of 50-250 µg/ml and cells were incubated for another 72 h. Medium was replaced by 100 µl of a fresh DMEM and 20 µl of the cell proliferation reagent. The absorbance at 490 nm was measured after 1 h for each well using a Safire II microplate reader (Tecan System Inc., Austria). The cell viability was calculated based on a comparison between absorbance values obtained for non-treated cells (a positive control) and cells incubated with nanoparticles using a standard one-way analysis of variance (ANOVA, mean (n=3), ±SD, three independent experiments).

Conclusions

Many different factors have to be considered while designing the nanosensor for intracellular imaging and sensing, including the size and charge of the nanoparticles, the method of delivering the nanoparticles to the specific cell line as well as the influence of the nanomaterial on the cellular environment.[11] Silica nanoparticles doped with oxygen-sensitive $[Ru(dpp)_3]^{2+}$ complex described in this paper demonstrate a considerable potential in this area. A very monodispersed population of spherical nanoparticles with a size compatible with the intracellular application can be obtained relatively easily using our new modified Stöber method. Excellent reproducibility both from cycle to cycle and from batch to batch within the full dissolved oxygen concentration range is demonstrated for the extracellular calibration of nanoparticles in water. TEM analysis performed on U_2OS incubated with nanoparticles for 24 h and 48 h revealed the endosomal lysosomal trafficking of nanoparticles. Quantitative results from the intracellular measurements were obtained on the FD FLIM. The intracellular dissolved oxygen concentration obtained for respiring cells is equal to 7.8 ppm, value which is in an agreement with the literature. An overall decrease in the nanosensor performance was detected when nanoparticles were incubated with cells compared to that obtained for nanoparticles dispersed in water which is likely due to the coating of the nanoparticle surface with proteins present in the biological environment. A decrease in the lifetime from ~ 4.4 µs to ~ 3.3 µs was observed within the dissolved oxygen concentration range. This change in lifetime is smaller in comparison to what was detected on the phase fluorometry setup for the nanoparticles dispersed in water. It was also established using standard colorimetric method that the nanoparticles showed no cytotoxic effect on the cell line used in this study. The results obtained from this work are very promising, however to fully evaluate the real potential of the nanoparticles for their in vivo application, further investigations need to be performed where the time the nanoparticles remain in the cell and how cells might respond to these nanoparticles over the longer incubation period should be determined.

Acknowledgements

This work is supported by a Higher Education Authority (HEA) grant to the Targeted Therapeutics and Theranostics (T3) Programme at DCU under Programme for Research in Third-Level Institutions (PRTLI) IV. Part of this work was performed in the frame of the Proof of Concept Studies for the ESFRI research infrastructure project Euro-BioImaging at the PCS FLIM facility located at The Netherlands Cancer Institute. The assistance of Mrs Tiina O´Neill, UCD Conway Institute of Biomolecular and Biomedical Research, with TEM imaging is gratefully acknowledged. The authors would like also to acknowledge the assistance of Ms. Claire O'Connell, School of Physics, Dr. Jose Manuel Hierrezuelo Osorio and Dr. Dermot Brougham, School of Chemistry, DCU with DLS measurements.

Notes and references

[a] Optical Sensors Laboratory, School of Physical Sciences, Biomedical Diagnostics Institute, Dublin City University, Glasnevin, Dublin 9, Ireland.

[b] Department of Cell Biology, The Netherlands Cancer Institute, Plesmanlaan 121, 1066CX Amsterdam, Netherlands.

† Electronic Supplementary Information (ESI) available. See DOI: 10.1039/xxxxxxx/

1 F. J. Giordano, *J. Clin. Invest.,* 2005, **115**, 500-8.
2 K. J. A. Davies, *Biochem. Soc. Symp*., 1995, **61**, 1–31.
3 S. Lahiri, C. Rozanov, A. Roy, B. Storey, D. G. Buerk, *Int. J. Biochem. Cell Biol*., 2001, **33**, 755-774.
4 G. L. Semenza, *Science,* 2007, **318**, 62-64.
5 B. Uttara, A. V. Singh, P. Zamboni, R. T. Mahajan, *Curr. Neuropharmacol*., 2009, **7**, 65-74.
6 T. Labasque, C. Chaumery, A. Aminot, G. Kergoat, *Mar. Chem*., 2004, **88**, 53-60.
7 L. C. Clark, *Trans. Am. Soc. Artif. Intern. Organs*, 1956, **2**, 41-48.
8 C. McDonagh, C. S. Burke, B. D. MacCraith, *Chem. Rev. (Washington, DC, U.S.)*, 2008, **108**, 400-422.
9 H. Xu, J. W. Aylott, R. Kopelman, T. J. Miller, M. A. Philbert, *Anal. Chem*., 2001, **73**, 4124-4133.
10 Y. E: L. Koo, Y. F. Cao, R. Kopelman, S. M. Koo, M. Brasuel, M. A. Philbert, *Anal. Chem*., 2004, **76**, 2498-2505.
11 A. Fercher, S. M. Borisov, A. V. Zhdanov, I. Klimant, D. B. Papkovsky, *ACS Nano,* 2011, **5**, 5499-5508.
12 Y-E. K. Lee, E. E. Ulbrich, G. Kim, H. Hah, C. Strollo, W. Fan, R. Guriar, S. Koo, R. Kopelman, *Anal. Chem*., 2010, **82**, 8446-8455.
13 A. Fercher, T. C. O'Riordan, A. V. Zhdanov, R. I. Dmitriev, D. B. Papkovsky, *Methods Mol. Biol. (Totowa, NJ, U.S.)*, 2010, **591**, 257-273.
14 R. I. Dmitriev, A. V. Zhdanov, G. V. Ponomarev, D. V. Yashunski,, D. B. Papkovsky, *Anal. Biochem*., 2010, **398**, 24-33.
15 T. V. Esipova, A. Karagodov, J. Miller, D. F. Wilson, T. M. Busch, S. A. Vinogradov, *Anal. Chem*., 2011, **83**, 8756-8765.
16 S. M. Borisov, D. L. Herrod, I. Klimant, *Sens. Actuators, B*, 2009, **139**, 52-58.
17 B. Korzeniowska, R. Nooney, D. Wencel, C. McDonagh, *Nanotechnology,* 2013, **24**, 442002.
18 X.-D. Wang, J. A. Stolwijk, T. Lang, M. Sperber, R. J. Meier,;J. Wegener, O. S. Wolfbeis, *J. Am. Chem. Soc*., 2012, **134**, 17011-17014.
19 C. He, W. Zhu, Y. Xu, Y. Zhong, J. Zhou, X. Qian, *J. Mater. Chem*., 2010, **20**, 10755-10764.
20 A. V. Kondrashina, R. I. Dmitriev, S. M. Borisov, I. Klimant, I. O'Brien, Y. M. Nolan, A. V. Zhdanov, D. B. Papkovsky, *Adv. Funct. Mater.*, 2012, **22**, 4931-4939.
21 X.-H. Wang, H.-S. Peng, H. Ding, F.-T. You, S.-H. Huang, F. Teng, B. Dong, H. W. Song, *J. Mater. Chem*., 2012, **22**, 16066-16071.
22 E. Ruoslahti, S. N. Bhatia, M. J. Sailor, *J. Cell Biol*., 2010, **188**, 759-768.
23 H. A. Clark, M. Hoyer, M. A. Philbert, R. Kopelman, *Anal. Chem*., 1999, **71**, 4831-4836.
24 A. Burns, H. Ow, U. Wiesner, *Chem. Soc. Rev.*, 2006, **35**, 1028-1042.
25 Y.-P. Chen, H.-A. Chen, Y. Hung, F.-C. Chien, P. Chen, C.-Y. Mou, *RSC Adv.*, 2012, **2**, 968-973.
26 B. Korzeniowska, R. Woolley, J. DeCourcey, D. Wencel, C.-E. Loscher, C.. McDonagh, *J. Biomed. Nanotechnol.*, 2014, **10**, 1336-1345.
27 H. A. Clark, R. Kopelman, R. Tjalkens, M. A. Philbert, *Anal. Chem*., 1999, **71**, 4837-4843.
28 A. Schulz, R. Woolley, T. Tabarin, C. McDonagh, *Analyst (Cambridge, U.K.)*, 2011, **136**, 1722-1727.
29 X. Hun, Z. Zhang, *Microchim. Acta*, 2007, **159**, 255-261.
30 L. Bau, F. Selvestrel, M. Arduini, I. Zamparo, C. Lodovichi, F. Mancin, *Org. Lett.*, 2012, **14**, 2984-2987.
31 P. Teolato, E. Rampazzo, M. Arduini, F. Mancin, P. Tecilla,;U. Tonellato, *Chemistry*, 2007, **13**, 2238-2245.
32 S. Bonacchi, E. Rampazzo, M. Montalti, L. Prodi, N. Zaccheroni, F. Mancin, P. Teolato, *Langmuir*, 2008, **24**, 8387-8392.
33 S. Seo, H. Y. Lee, M. Park, J. M. Lim, D. Kang, J. Yoon, J. H. Jung, *Eur. J. Inorg. Chem.*, 2010, **6**, 843-847.
34 C. Zong, K. Ai, G. Zhang, H. Li, L. Lu, *Anal. Chem*., 2011, **83**, 3126-3132.
35 E. Rampazzo, S. Bonacchi, D. Genovese, R. Juris, M. Sgarzi, M. Montalti, L. Prodi, N. Zaccheroni, G. Tomaselli, S. Gentile *et al.*, *Chemistry*, 2011, **17**, 13429-13432.
36 G. Kim, Y.-E. K. Lee, H. Xu, M. A. Philbert, R. Kopelman, *Anal. Chem*., 2010, **82**, 2165-2169.
37 W.-K. Oh, Y. S. Jeong, S. Kim, J. Jang, *ACS Nano*, 2012, **6**, 8516-8524.
38 R. Woolley, S. Roy, U. Prendergast, A. Panzera, L. Basabe-Desmonts, D. Kenny, C. McDonagh, *Nanomedicine: Nanotech. Biol. Med*., 2013, **9**, 540-549.
39 M. C. Estevez, M. B. O'Donoghue, X. Chen, W. Tan, *Nano Res.*, 2009, **2**, 448-461.
40 S. M. Borisov, I. Klimant, *Microchim. Acta*, 2009, **164**, 7-15.
41 A. Lapresta-Fernandez, T. Doussineau, S. Dutz, F. Steiniger, A. J. Moro, G. J. Mohr, *Nanotechnology*, 2011, **22**, 415501.
42 F. Zhang, Z. Ali, F. Amin, A. Riedinger, W. J. Parak, *Anal. Bioanal. Chem.*, 2010, **397**, 935-942.
43 M. T. Chen, L. M. Gomez, F. N. Ishikawa, P. T. Vernier, C. Zhou, M. A. Gundersen, *Nanotechnology*, 2009, **20**, 295101.
44 C.-P. Tsai, C.-Y. Chen, Y. Hung, F.-H. Chang, C.-Y. Mou, *J. Mater. Chem.*, 2009, **19**, 5737-5743.
45 T. Schiestel, H. Brunner, G. E. M. Tovar, *J. Nanosci. Nanotechnol.*, 2004, **4**, 504-511.
46 X. J. Zhao, R. Tapec-Dytioco, W. H. Tan, *J. Am. Chem. Soc.*, 2003, **125**, 11474-11475.
47 S. Santra, P. Zhang, K. M. Wang, R. Tapec, W. H. Tan, *Anal. Chem*., 2001, **73**, 4988-4993.
48 J. W. Aylott, *Analyst (Cambridge, U.K.)*, 2003, **128**, 309-312.
49 G. Bhakta, R. K. Sharma, N. Gupta, S. Cool, V. Nurcombe, A. Maitra, *Nanomedicine: Nanotech. Biol. Med*., 2011, **7**, 472-479.
50 J. Lu, M. Liong, Z. Li, J. I. Zink, F. Tamanoi, *Small*, 2010, **6**, 1794-1805.

51 C. McDonagh, B. D. MacCraith, A. K. McEvoy, *Anal. Chem*., 1998, **70**, 45-50.
52 M. J. Moreno, E. Monson, R. G. Reddy, A. Rehemtulla, B. D. Ross, M. Philbert, R. J. Schneider, R. Kopelman, *Sens. Actuators, B*, 2003, **90**, 82-89.
53 J. R. Bacon, J. N. Demas, *Anal. Chem.*, 1987, **59**, 2780-2785.
54 E. R. Carraway, J. N. Demas, B. A. Degraff, *Anal. Chem.*, 1991, **63**, 332-336.
55 W. Y. Xu, R. C. McDonough, B. Langsdorf, J. N. Demas, B. A. Degraff, *Anal. Chem.*, 1994, **66**, 4133-4141.
56 A. B. Mohseny, I. Machado, Y. Cai, K.-L. Schaefer, M. Serra, P. C. W. Hogendoorn, A. Llombart-Bosch, A. M. Cleton-Jansen, *Lab. Invest.*, 2011, **91**, 1195-1205.
57 R. I. Dmitriev, D. B. Papkovsky, *Cell. Mol. Life Sci.*, 2012, **69**, 2025-2039.
58 D. Wencel, C. Dolan, M. Barczak, T.E. Keyes, C. McDonagh, *Nanotechnology*, 2013, **24**, 365705.

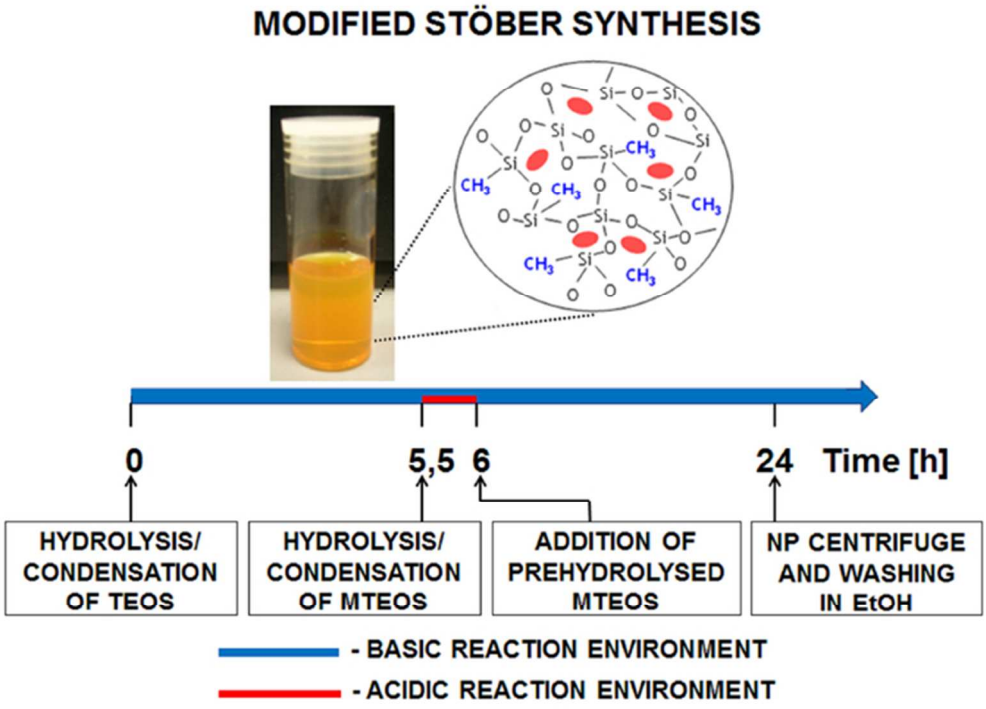

57x41mm (300 x 300 DPI)

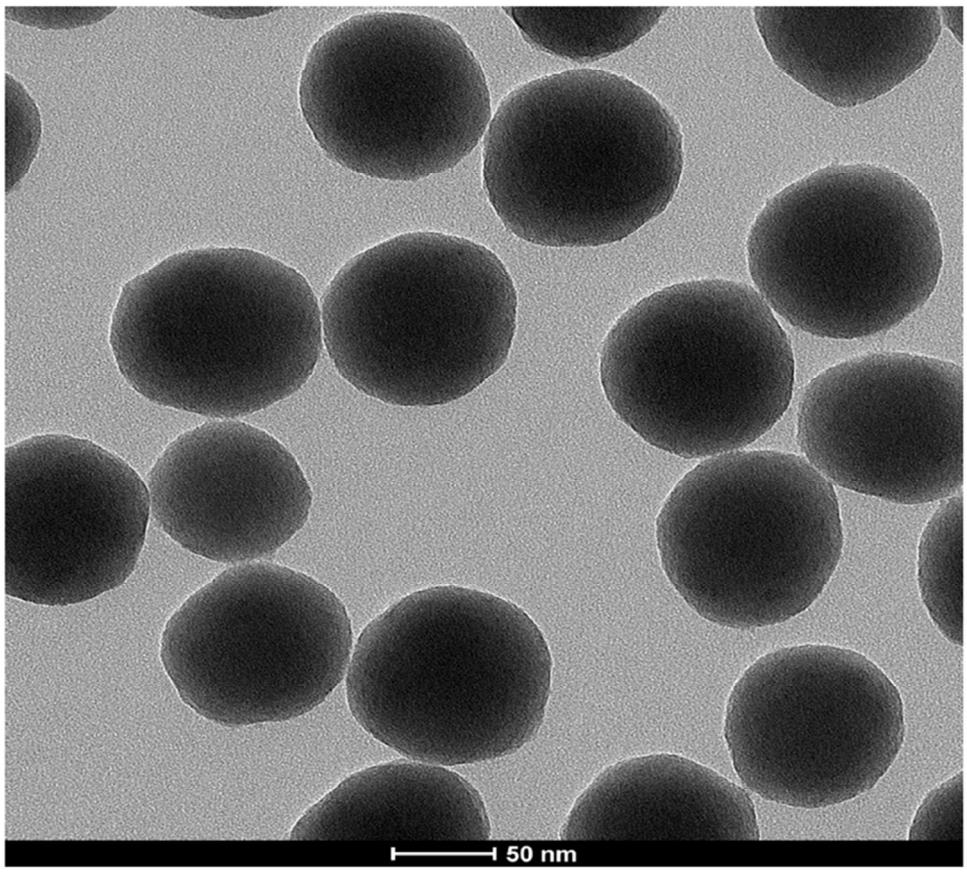

73x68mm (300 x 300 DPI)

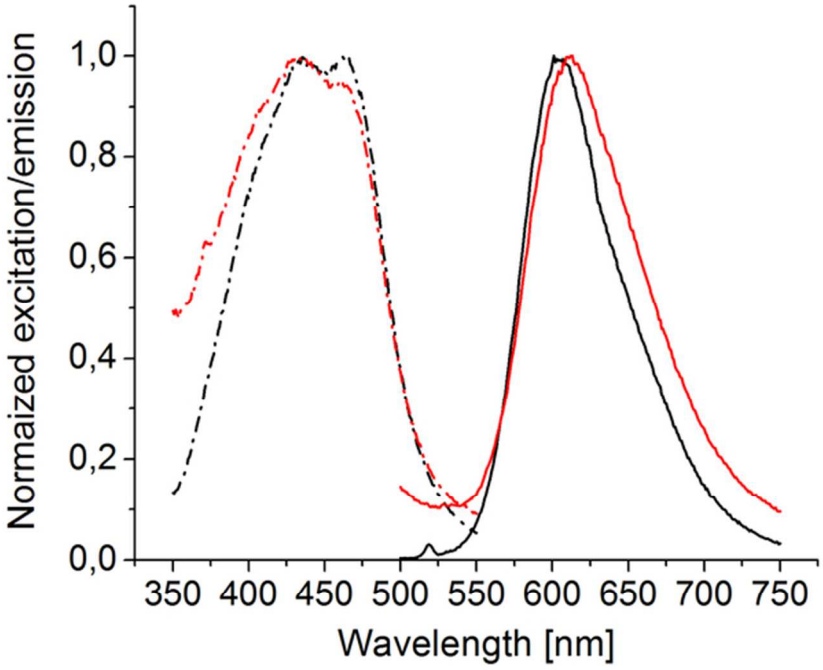

61x47mm (300 x 300 DPI)

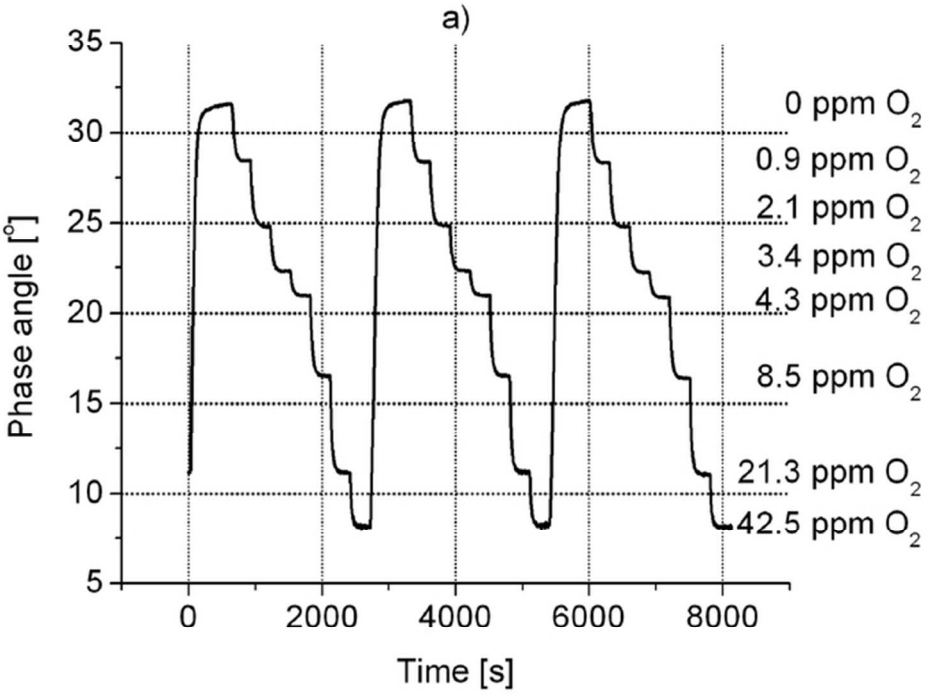

61x48mm (300 x 300 DPI)

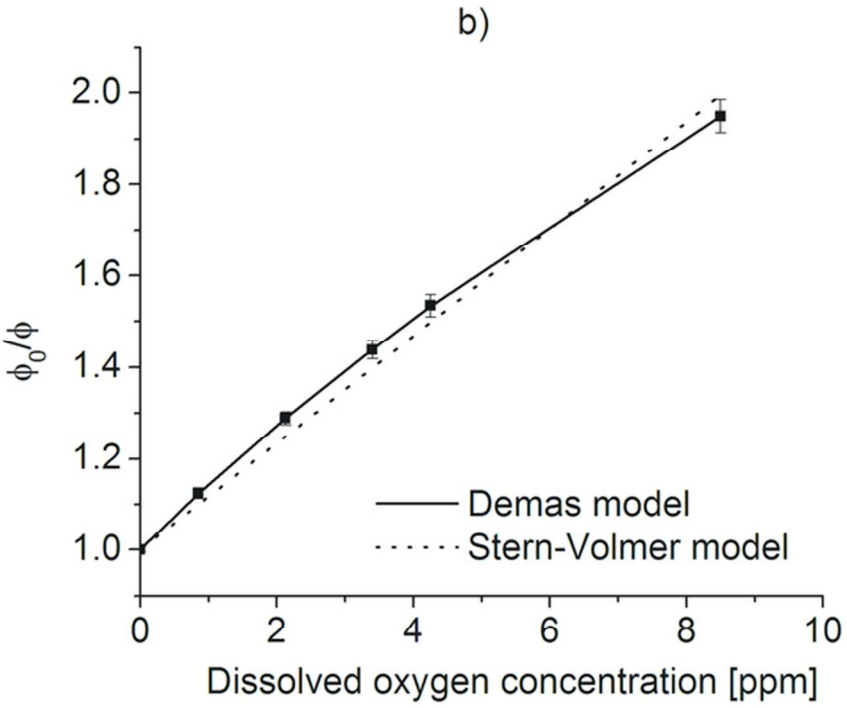

61x46mm (300 x 300 DPI)

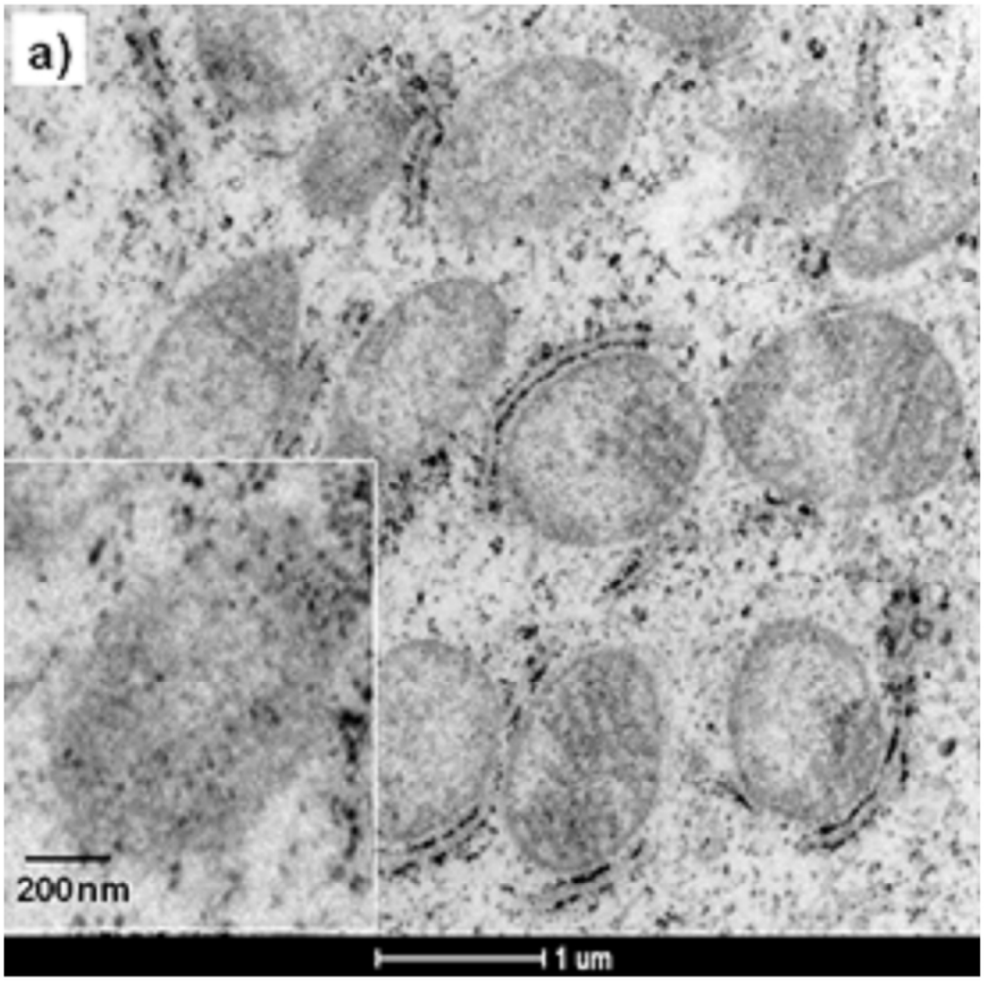

69x69mm (300 x 300 DPI)

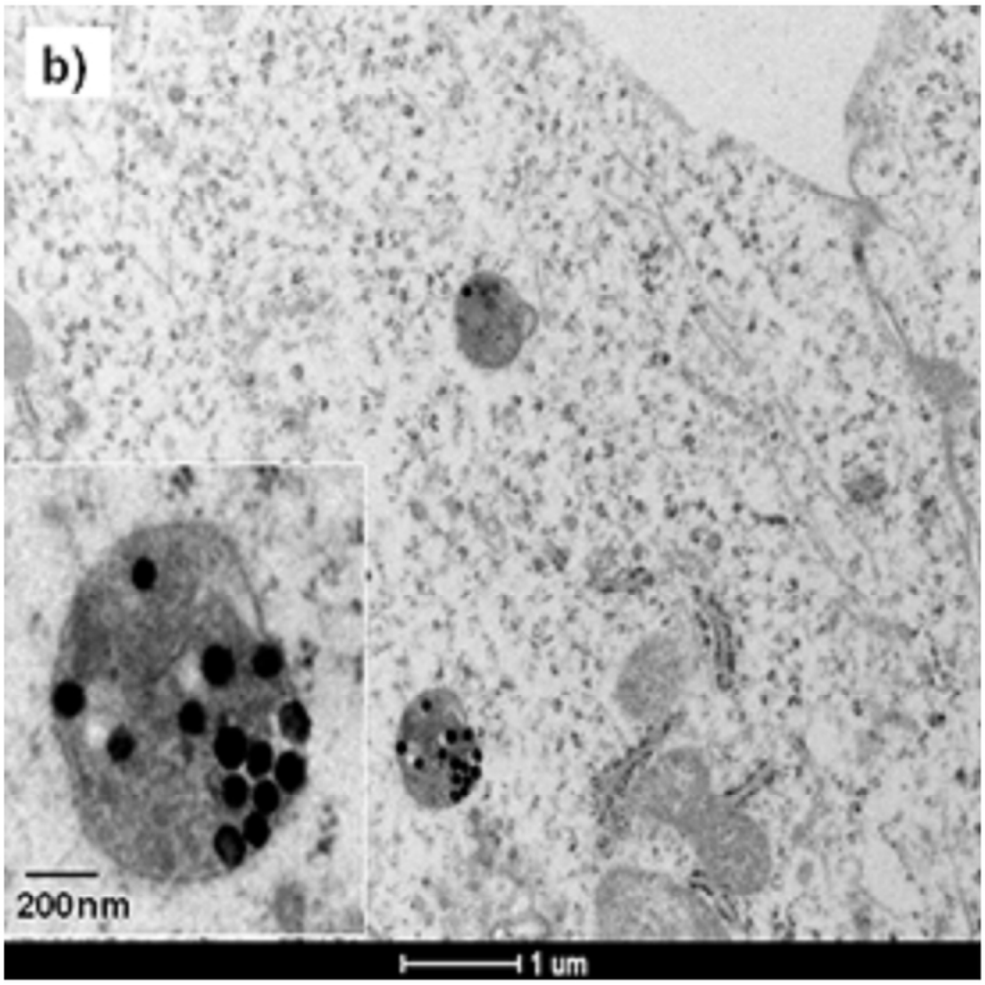

69x69mm (300 x 300 DPI)

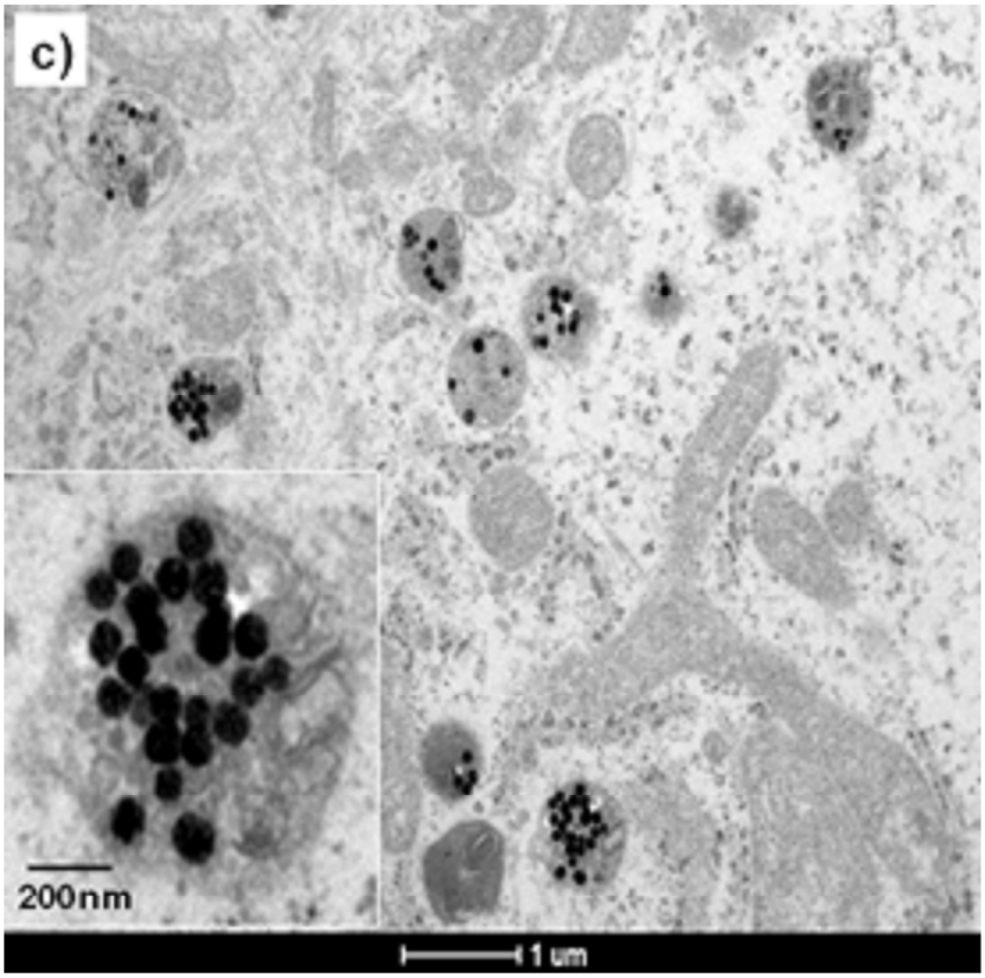

69x69mm (300 x 300 DPI)

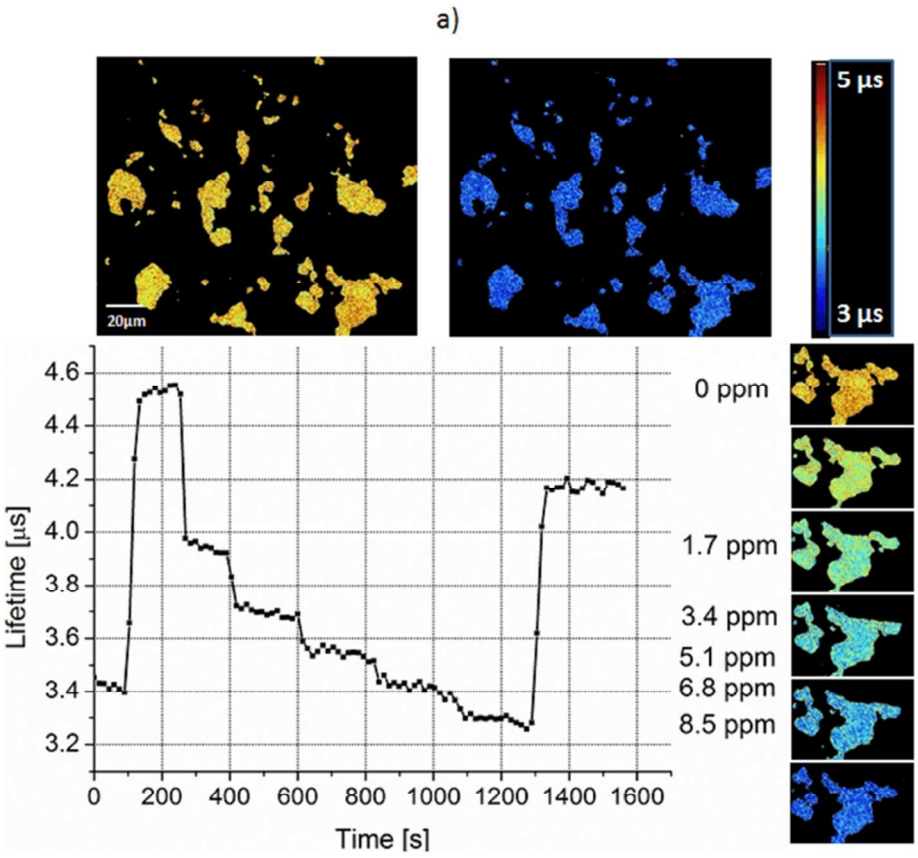

75x69mm (300 x 300 DPI)

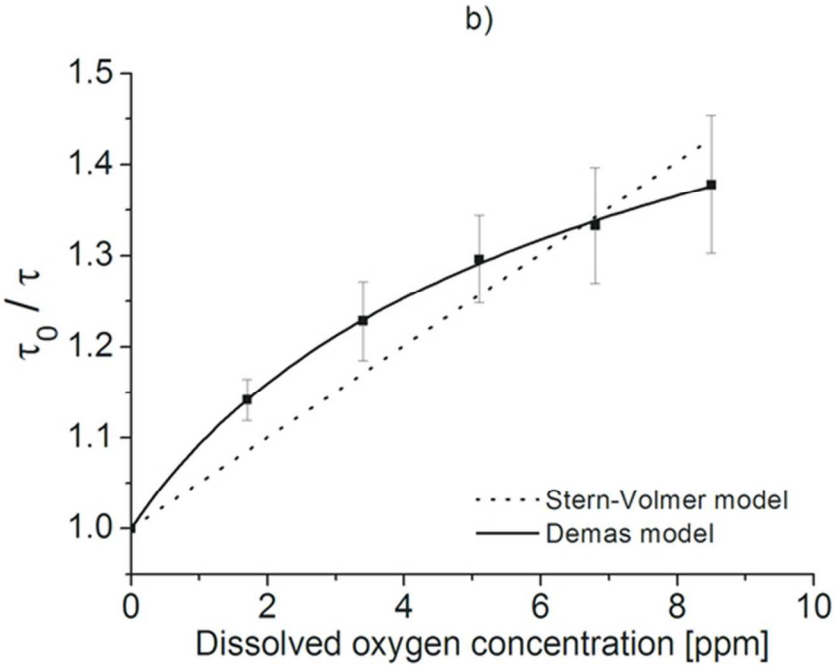

55x38mm (300 x 300 DPI)

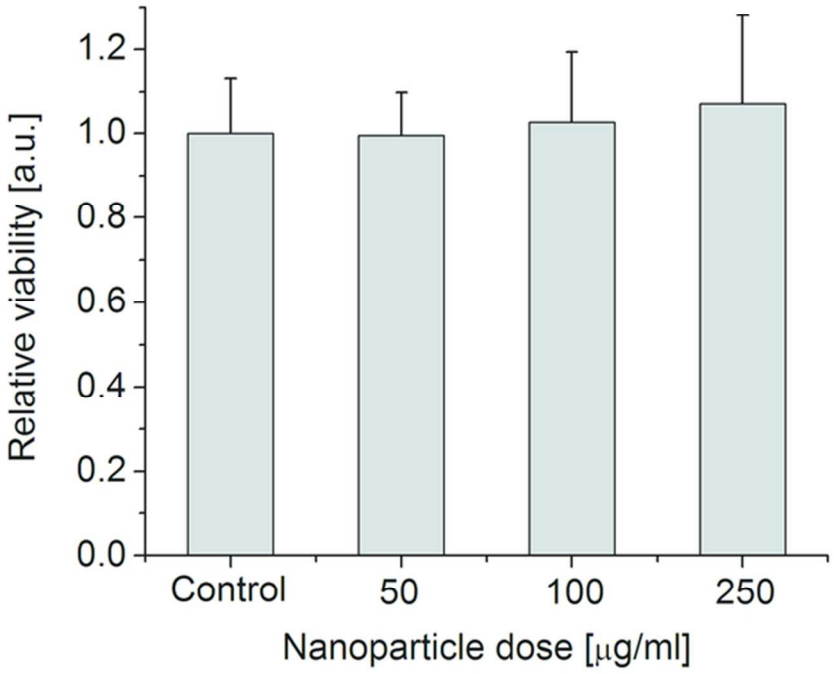

61x46mm (300 x 300 DPI)